Effects of Inorganic Oxides on Polymer Binder Burnout. II. Poly(butyl methacrylate)

AUROBINDO NAIR and ROBERT L. WHITE*

Department of Chemistry and Biochemistry, University of Oklahoma, Norman, Oklahoma 73019

SYNOPSIS

The effects of silica, mullite, α-alumina, and γ-alumina on the nonoxidative thermal degradation of poly(butyl methacrylate) are described. Under conditions similar to those employed for nonoxidative ceramic sintering, more volatile alkyl aromatic species were detected when polymer/oxide samples were heated than when the neat polymer was heated. Relative to the neat polymer, all of the inorganic oxides inhibited monomer evolution and promoted an ester decomposition reaction that yielded butene. Infrared analysis indicated that poly(methacrylic acid) segments resulting from ester decomposition reacted to form anhydride. The presence of water vapor during the thermal degradation of the neat polymer and polymer/oxide samples lowered the temperatures at which monomer evolution maximized but had little effect on butene evolution. When the polymer was coated on γ-alumina, significant amounts of carboxylate were formed above 400°C as a result of deprotonating poly(methacrylic acid) functionalities on the γ-alumina surface.

INTRODUCTION

Polymers are employed by the ceramics industry as inorganic oxide binders to form green bodies that are subsequently fired to produce ceramic products. Ideally, polymer binders decompose (burnout) during the early stages of ceramic sintering. Although complete decomposition can usually be achieved in oxidative burnout atmospheres, incomplete binder decomposition may be obtained in inert or reductive atmospheres. Nonoxidative binder burnout is often required in the production of ceramic integrated circuit substrates to avoid oxidation of cofired metals.[1-5] It is known that inorganic oxides can interact with polymer binders during binder burnout and that these interactions affect binder thermal degradation.[6-13] If significant quantities of polymer residue remain above temperatures at which ceramic sintering begins, flaws in ceramic end products may result. It is, therefore, useful to examine the effect of inorganic oxides on the nonoxidative thermal degradation of polymer binders used in electronics industry applications.

Poly(butyl methacrylate) (PBMA) is a popular ceramic binder used by the microelectronics industry because it decomposes at relatively low temperatures in nonoxidative environments. In addition, PBMA can be applied in aqueous emulsions so that the environmental impact of large-scale manufacturing is minimized when this polymer is employed. Commercial grade PBMA is prepared by free-radical polymerization of butyl methacrylate. The reaction is initiated by peroxide or azo compounds and can terminate in two ways. Radical combination yields chains with head-to-head linkages, whereas disproportionation results in polymer chains with saturated and vinylidene end groups.[14,15] The least thermally stable linkages in neat PBMA are the head-to-head linkages.[14,16-18] Butyl methacrylate can be produced at relatively low temperatures by polymer unzipping after head-to-head linkage cleavage:[16,19]

* To whom correspondence should be addressed.

Journal of Applied Polymer Science, Vol. 60, 1911–1920 (1996)
 CCC 0021-8995/96/111911-10

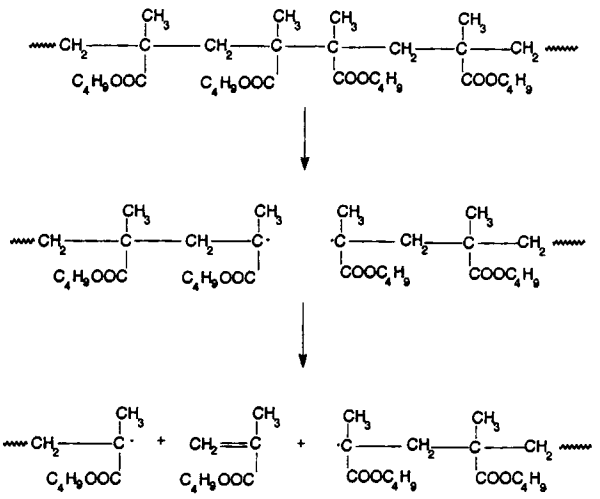

At higher temperatures, PBMA decomposes by unzipping after β-scission at vinylidene chain ends:[14,16–18]

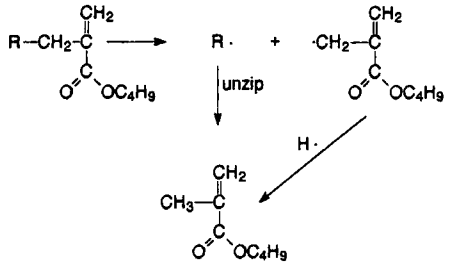

A third thermal degradation process, which is typically the principal degradation reaction,[14,16,17,20–22] involves random chain scission followed by β-scission to yield butyl methacrylate.

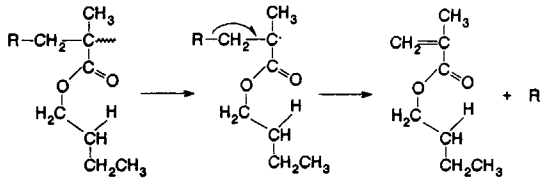

In addition, PBMA may undergo ester decomposition to form methacrylic acid polymer segments and butene.

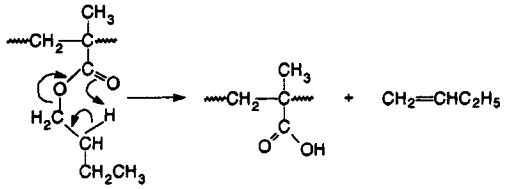

Acid polymer segments formed by this process may subsequently undergo dehydration to yield an anhydride.[23]

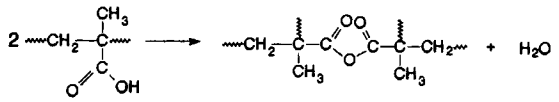

EXPERIMENTAL

Apparatus

The instruments and conditions employed for pyrolysis-GC/MS, thermogravimetry–mass spectrometry (TG–MS), and variable temperature diffuse reflectance Fourier transform infrared spectroscopy (VT-DRIFTS) studies are described in the preceding article.[13]

Samples

Silica, mullite, and commercial grade PBMA (MW $2–3 \times 10^5$) were obtained from Hitachi (Hitachi City, Japan), α-alumina was purchased from Aldrich Chemical Co. (Milwaukee, WI), γ-alumina was purchased from Johnson Matthey/AESAR (Seabrook, NH), and 2-propanol was purchased from J. T. Baker Inc. (Phillipsburg, NJ). Helium (99.9995%) was purchased from Union Carbide Corp., Linde Division (Danbury, CT). Particle size ranges, surface areas, and hydroxyl contents for the inorganic oxides used in this study are listed in the preceding article.[13] Approximately 10% (wt/wt) PBMA/oxide samples were prepared by dissolving 1.7 g of PBMA in 250 mL of 2-propanol, adding 25 mL of this solution to 1.5 g of oxide, and rotoevaporating the mixture to remove the solvent.

RESULTS

By using pyr-GC/MS, thermal degradation products formed by rapidly heating neat PBMA and PBMA/oxide samples to 500°C were identified. As shown in Table I, the dominant neat PBMA decomposition process at 500°C led to butyl methacrylate formation. Butene and methacrylic acid detected by pyr-GC/MS likely resulted from ester decomposition. An unsaturated ester, water, benzene, alkyl aromatics, and methyl methacrylate were also detected as volatile products, but at very low levels. Like neat PBMA, the major volatile product generated by pyrolysis of

Table I Neat PBMA and PBMA/oxide pyr-GC/MS Products at 500°C

Relative Abundance (%)	PBMA Sample				
	Neat PBMA	Silica	Mullite	α-Alumina	γ-Alumina
Butene	6.8[a]	12.0	16.7	15.8	38.0
Unsaturated ester	0.2	0.4	0.3	0.3	0.7
H_2O	0.1	0.8	0.9	0.4	3.0
Benzene	0.1	0.6	0.5	0.4	0.6
Alkyl aromatics	0.1	0.2	0.3	0.3	0.5
Methyl methacrylate	0.3	0.1	0.2	0.1	0.2
Butyl methacrylate	82.6	75.6	72.4	73.8	47.2
Methacrylic acid	5.8	5.1	3.6	0.9	1.0

[a] Percentage of integrated total ion current.

the PBMA/oxide samples was butyl methacrylate. However, the relative amount of butyl methacrylate evolved from the PBMA/oxide samples was less than that from neat PBMA. The relative amount of butyl methacrylate generated by pyrolysis was the least for the PBMA/γ-alumina sample, but this sample yielded significantly more butene than the other samples. Compared to neat PBMA pyrolysis, more butene was generated by pyrolysis of the PBMA/oxide samples at 500°C. These findings suggest that ester decomposition was promoted by the oxides, especially for the PBMA/γ-alumina sample. The ester decomposition reaction also gave rise to methacrylic acid polymer segments, as evidenced by the methacrylic acid detected after depolymerization of these polymer regions. However, although more butene was detected for the PBMA/oxide samples than for neat

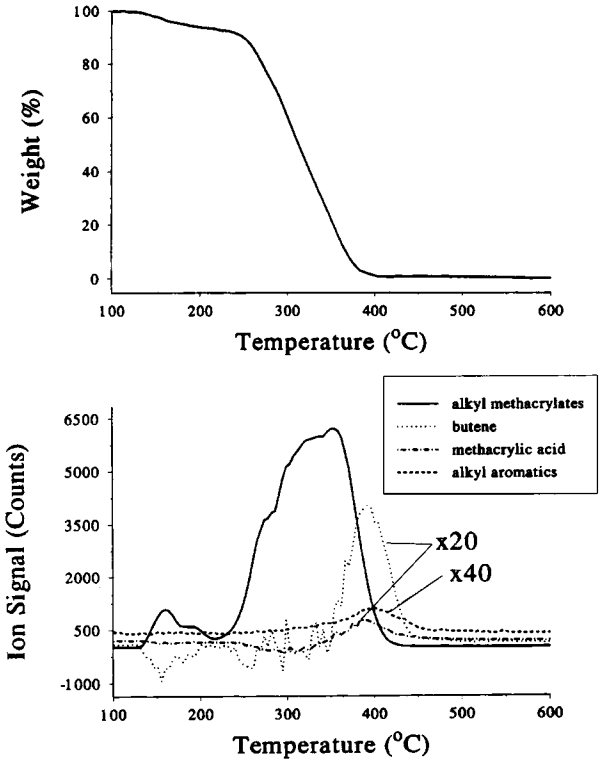

Figure 1 Weight loss curve and ion signal temperature profiles obtained by TG–MS analysis of neat PBMA.

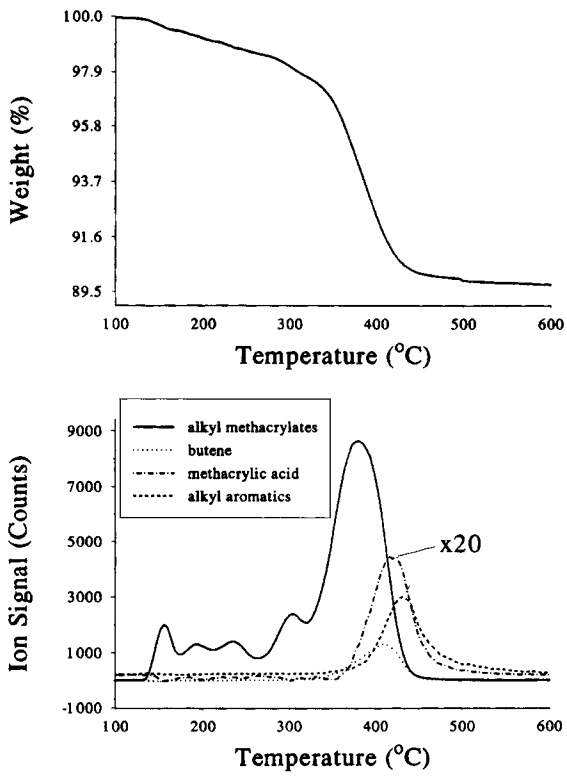

Figure 2 Weight loss curve and ion signal temperature profiles obtained by TG–MS analysis of a PBMA/silica sample.

PBMA, a correspondingly larger amount of methacrylic acid was not detected in the volatile pyrolysis products denrived from the PBMA/oxide samples, suggesting that the methacrylic acid polymer segments formed by ester decomposition may have undergone further reactions. The large amount of water generated by pyrolysis of the PBMA/γ-alumina sample was consistent with the fact that the γ-alumina used in this study contained significantly more hydroxyls than the other oxides.[13]

Neat PBMA and PBMA/oxide samples were analyzed by TG–MS to examine binder burnout processes under conditions that were similar to those employed for ceramic sintering. TG–MS ion signal temperature profiles were generated for butene (m/z 56), alkyl methacrylates (m/z 69), methacrylic acid (m/z 86), and alkyl aromatics (m/z 91). The m/z 69 ion was the most intense ion formed by electron bombardment of butyl methacrylate. Because the m/z 56 and m/z 86 ions representing butene and methacrylic acid were also present in neat butyl methacrylate mass spectra, ion signal temperature profiles representing butene and methacrylic acid were obtained after subtracting the ion intensity contributions from butyl methacrylate from the selected ion intensities. The 56/69 and 86/69 ion intensity ratios found in neat butyl methacrylate mass spectra were used as subtraction factors. Butyl methacrylate contributions to m/z 56 and m/z 86 ion intensities were removed from TG–MS mass spectra by multiplying the m/z 69 ion intensity by the subtraction factors and then subtracting the resulting values from the m/z 56 and m/z 86 ion intensities.

Figure 1 shows the weight loss curve and species specific ion signal temperature profiles obtained by TG–MS analysis of neat PBMA. PBMA weight loss was complete at about 400°C. The alkyl methacrylates ion signal temperature profile for neat PBMA degradation exhibited multiple peaks, which is consistent with previous studies.[16,17] The first depolymerization step occurred at approximately 150°C and was attributed to head-to-head linkage cleavage. The increase in the alkyl methacrylates ion signal near 225°C was attributed to depolymerization after cleavage of vinylidene chain ends. The broad depolymerization step centered near 350°C was attributed to random chain cleavage. The maximum of the methacrylic acid ion signal was coincident with the butene ion signal temperature profile maximum and occurred at about 385°C. The maximum for the alkyl aromatics ion signal temperature profile occurred at about 410°C.

Figure 2 shows the weight loss curve and species specific ion signal temperature profiles for a PBMA/silica sample obtained by TG–MS analysis. Weight loss for the PBMA/silica sample occurred in a series of small steps up to about 325°C. The most significant weight loss was detected above 325°C. The alkyl methacrylates ion signal temperature profile comprised five overlapping peaks and the peak at about 380°C was the largest of the five. In contrast, ion signal temperature profiles for butene, methacrylic acid, and alkyl aromatics exhibited single peaks. The methacrylic acid ion signal peak maximum was coincident with the butene ion signal temperature profile maximum and occurred at about 410°C. The maximum for the alkyl aromatics ion signal temperature profile occurred at about 440°C.

Figure 3 shows the weight loss curve and species specific ion signal temperature profiles for a PBMA/mullite sample. Weight loss for the PBMA/mullite sample occurred in three steps that began at about 160, 260, and 320°C. Weight loss was complete at about 425°C. The alkyl methacrylates ion signal temperature profile comprised three overlapping peaks that corresponded to the three weight loss steps. Unlike the alkyl methacrylates ion signal profile, the methacrylic acid, butene, and alkyl aromatics ion signal temperature profiles exhibited

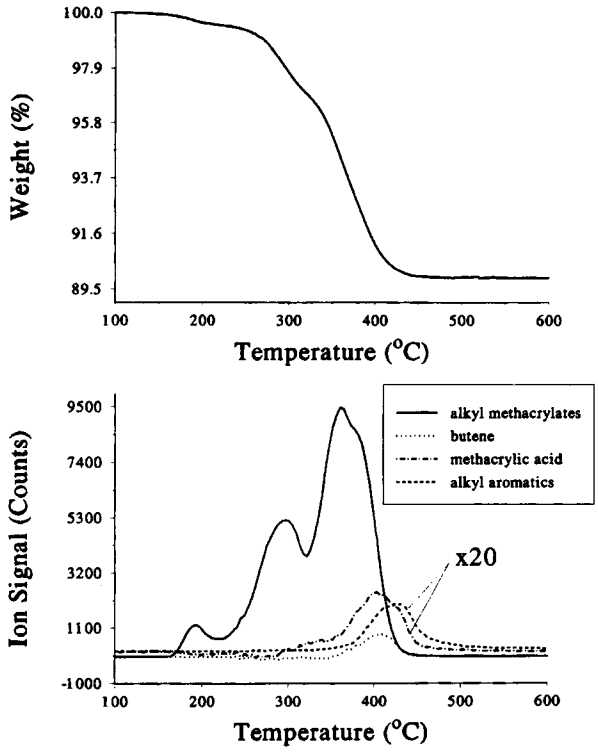

Figure 3 Weight loss curve and ion signal temperature profiles obtained by TG–MS analysis of a PBMA/mullite sample.

single peaks. Like the PBMA/silica sample, the maximum for the methacrylic acid ion signal occurred at about 410°C and was coincident with the butene ion signal temperature profile maximum and the maximum for the alkyl aromatics ion signal temperature profile occurred at about 440°C.

Figure 4 shows the weight loss curve and ion signal temperature profiles for a PBMA/α-alumina sample. Weight loss for the PBMA/α-alumina sample occurred in five steps that began at about 125, 170, 225, 275, and 340°C. Weight loss was complete at about 410°C. The alkyl methacrylates ion signal temperature profile contained five overlapping peaks that corresponded to the five weight loss steps. The ion signal temperature profiles for methacrylic acid, butene, and alkyl aromatic species exhibited single peaks. Like the PBMA/silica and PBMA/mullite samples, the PBMA/α-alumina sample methacrylic acid ion signal maximum was coincident with the butene ion signal temperature profile maximum. The maximum for the alkyl aromatics ion signal temperature profile occurred at about 420°C.

Figure 5 shows the weight loss curve and ion signal temperature profiles for a PBMA/γ-alumina sample. Weight loss for the PBMA/γ-alumina sample occurred throughout the TG–MS temperature ramp. However, the most significant weight loss was detected between 350–430°C. A single peak in the alkyl methacrylates ion signal temperature profile at about 400°C corresponded to this weight loss step. The butene ion signal temperature profile was comprised of two asymmetric peaks, the largest peak maximizing near 360°C. The methacrylic acid ion signal temperature profile exhibited a single peak that also maximized near 360°C. The alkyl aromatics ion signal temperature profile exhibited a maximum near 420°C, but the ion signal remained high for the remainder of the TG–MS heating ramp.

Water vapor is often added to nonoxidative sintering atmospheres to utilize the water gas reaction to remove carbon that forms during binder burnout. To ascertain the effects of water vapor on PBMA binder burnout processes, the previously described TG–MS experiments were repeated while purging samples with helium that had been saturated with water vapor. TG–MS results obtained in this manner were found to be similar to those derived from measurements for which dry helium was employed for sample purging, but the temperatures at which

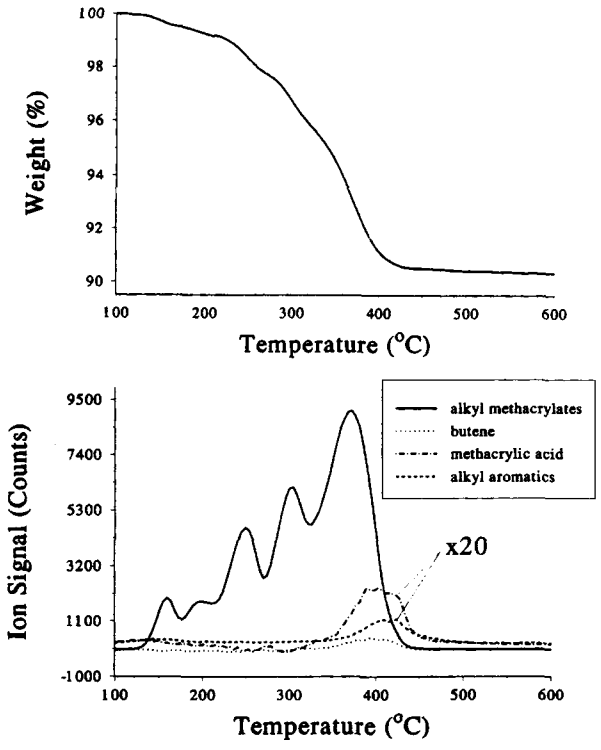

Figure 4 Weight loss curve and ion signal temperature profiles obtained by TG–MS analysis of a PBMA/α-alumina sample.

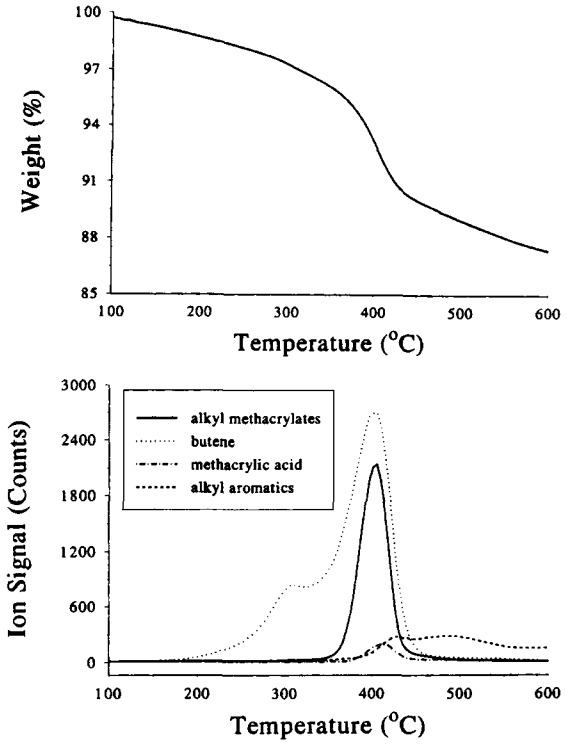

Figure 5 Weight loss curve and ion signal temperature profiles obtained by TG–MS analysis of a PBMA/γ-alumina sample.

volatile product evolutions maximized were somewhat lower when water vapor was present (vide infra).

VT-DRIFTS was employed to monitor functional group changes in the PBMA/oxide sample residues during sample heating. Figure 6 shows integrated absorbance temperature profiles for the O—H stretching vibration (3800–3050 cm^{-1}) and C—H stretching vibration (3030–2765 cm^{-1}) absorbance regions. The O—H stretching vibration absorbance represented: oxide hydroxyls, adsorbed water, and polymer hydroxyls formed as a result of thermal degradation processes. The C—H stretching vibration absorbance was representative of the polymer only. The O—H stretching vibration integrated absorbance temperature profiles resembled those obtained by VT-DRIFTS analysis of the neat oxides and the C—H stretching vibration integrated absorbance profiles resembled the weight loss curves obtained by TG–MS analysis of the polymer/oxide samples. For the PBMA/silica sample, significant C—H absorbance loss occurred in the 380–480°C temperature range. For the PBMA/mullite sample, loss of C—H groups occurred between 280 and 480°C, whereas C—H stretching vibration absorbance loss for the PBMA/α-alumina sample occurred mainly between 300 and 450°C. For the PBMA/γ-alumina sample, C—H absorbance loss was detected above 320°C and continued throughout the VT-DRIFTS heating ramp.

The appearance of a 1765 cm^{-1} infrared absorbance band, which is characteristic of anhydride formation, was detected for all of the PBMA/oxide samples. Temperature profiles of the 1765 cm^{-1} absorbance band intensity are shown in Figure 7 for the PBMA/oxide samples. Because the 1765 cm^{-1} band overlapped with a much larger 1730 cm^{-1} band in VT-DRIFTS spectra, curvefitting[24] was employed to deconvolute the two bands and more accurately determine the 1765 cm^{-1} band intensity. To facilitate comparisons, all absorbances were scaled to the initial 1730 cm^{-1} C=O stretching vibration absorbance band intensity for each sample. For the PBMA/silica sample, the temperature corresponding to maximum absorbance (T_M) for the anhydride band occurred at about 460°C. The anhydride band T_M value for the PBMA/mullite sample was found

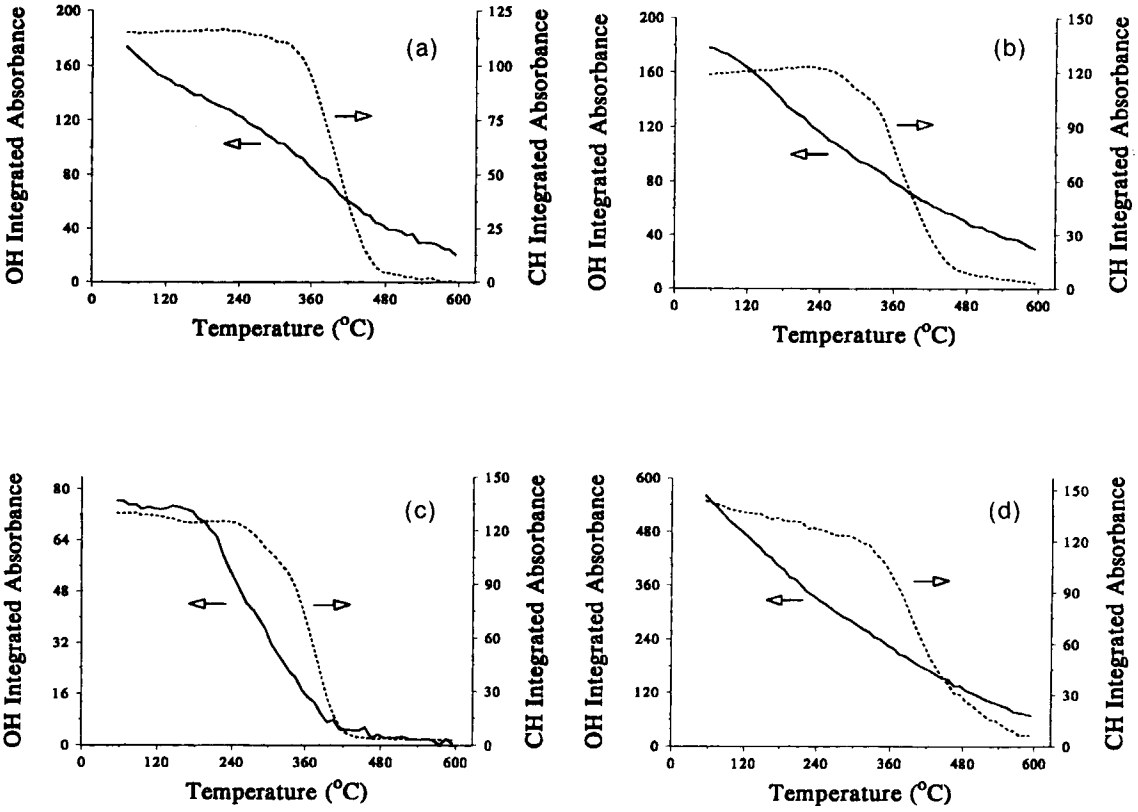

Figure 6 OH (3800–3050 cm^{-1}) and CH (3030–2765 cm^{-1}) integrated absorbance temperature profiles obtained by VT-DRIFTS analysis of (a) PBMA/silica, (b) PBMA/mullite, (c) PBMA/α-alumina, and (d) PBMA/γ-alumina samples.

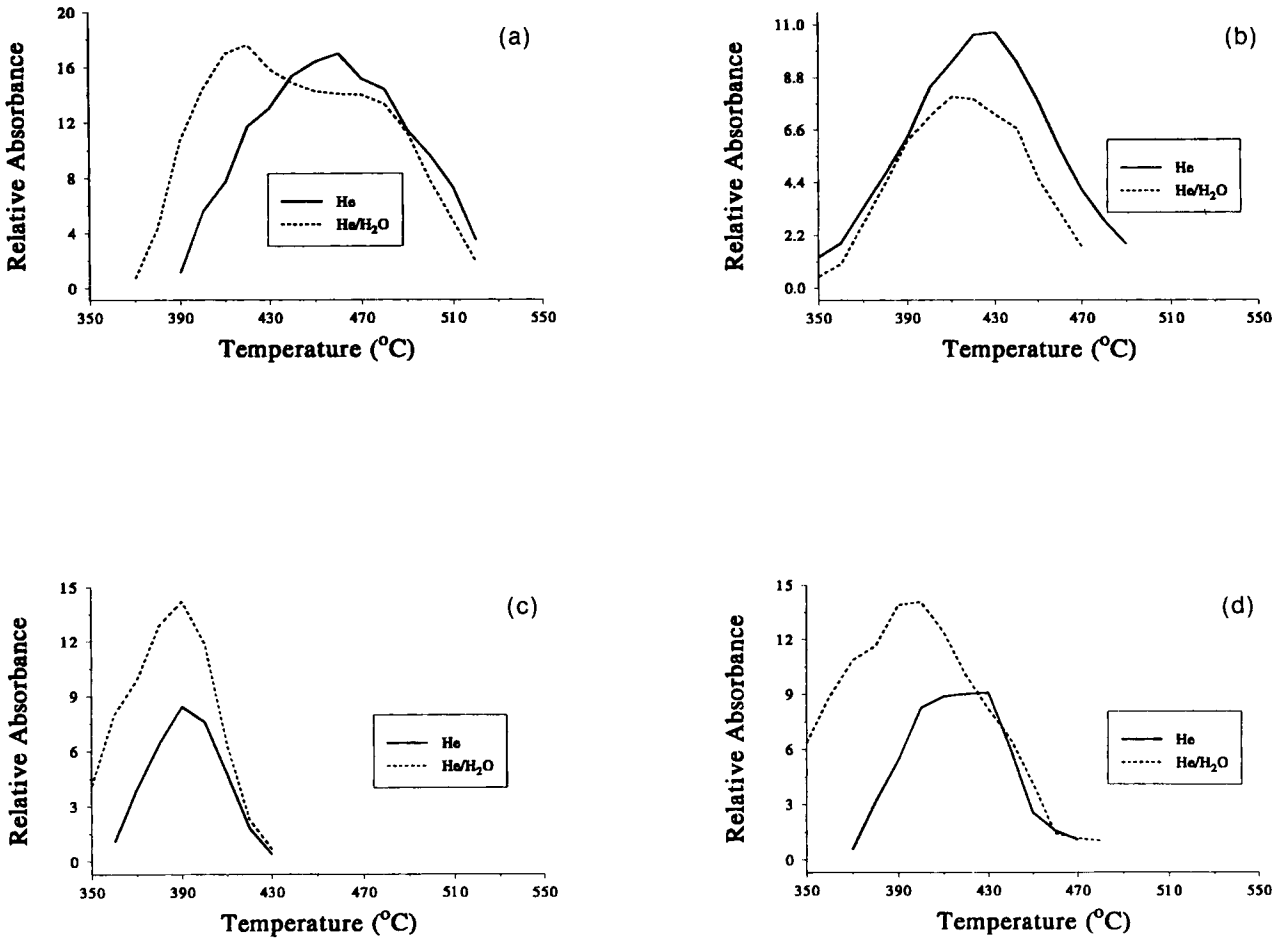

Figure 7 Anhydride 1765 cm^{-1} band intensity profiles obtained by VT-DRIFTS analysis of (a) PBMA/silica, (b) PBMA/mullite, (c) PBMA/α-alumina, and (d) PBMA/γ-alumina samples.

at about 430°C, whereas corresponding T_M values for the PBMA/α-alumina and PBMA/γ-alumina samples were 390 and 420°C, respectively. In the presence of water vapor, the anhydride band T_M value was reduced by 40°C for the PBMA/silica sample and by 20°C for both the PBMA/mullite and PBMA/γ-alumina samples. The anhydride band T_M value for the PBMA/α-alumina sample was not significantly affected by the presence of water vapor. However, the relative amount of anhydride formed by the PBMA/α-alumina and PBMA/γ-alumina samples increased in the presence of water vapor. For the PBMA/mullite sample, less anhydride was formed in the presence of water vapor, whereas for the PBMA/silica sample, the amount of anhydride formed was not significantly changed by the presence of water vapor.

VT-DRIFTS analysis of the PBMA/γ-alumina sample revealed a distinct infrared absorbance band at 1575 cm^{-1}, which is characteristic of carboxylate formation.[25] This band was not detected in VT-DRIFTS spectra obtained for neat PBMA or any of the other PBMA/oxide samples. The infrared absorbance temperature profile for the PBMA/γ-alumina carboxylate band is shown in Figure 8. The carboxylate band appeared in spectra at about 200°C and reached a maximum at about 470°C.

DISCUSSION

Pyr-GC/MS results (Table I) indicated that more butene was evolved from the PBMA/oxide samples than neat PBMA, suggesting that ester decomposition occurred more readily when PBMA was coated on the oxides. This was especially true for the PBMA/γ-alumina sample, for which the quantity of butene detected by pyrolysis at 500°C was almost as much as the amount of butyl methacrylate detected. The TG–MS butene evolution T_M value for the

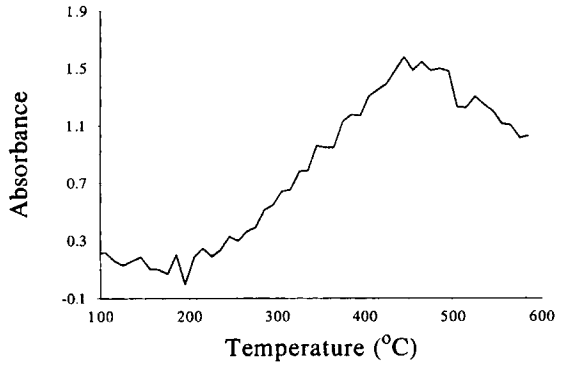

Figure 8 Carboxylate 1575 cm^{-1} band intensity profile obtained by VT-DRIFTS analysis of the PBMA/γ-alumina sample.

PBMA/γ-alumina sample was approximately 40°C lower than the butyl methacrylate evolution T_M value. In contrast, the butene evolution T_M values for the other PBMA/oxide samples were 20–30°C higher than those corresponding to butyl methacrylate evolution. Moreover, the TG–MS butene ion signal temperature profile for the PBMA/γ-alumina sample (Fig. 5) indicated that butene evolution occurred before significant amounts of monomer was detected, confirming that ester decomposition was promoted by γ-alumina. These results suggest that strong interactions between PBMA ester functionalities and γ-alumina weakened ester–butyl bonds and facilitated ester decomposition yielding butene.

With the exception of the PBMA/γ-alumina sample, PBMA weight loss occurred in a series of at least three steps, with the most prominent step being the last, which was likely due to unzipping after random chain scission. The fact that more than three monomer evolution peaks were detected for the PBMA/silica and PBMA/α-alumina samples suggests that the polymer coating for these samples was inhomogeneous or that multiple PBMA/oxide interactions affected polymer degradation for these samples. Interestingly, the butene and methacrylic acid ion signal temperature profiles for these samples did not exhibit multiple peaks, suggesting that the effect was restricted to monomer evolution processes. For the PBMA/silica and PBMA/mullite samples, sample weight loss was essentially complete at about 430°C, which was about 30°C higher than the corresponding temperature for neat PBMA. Weight loss ended for the PBMA/α-alumina sample at about 410°C. Weight loss for the PBMA/γ-alumina sample began immediately after heating the sample and continued throughout the TG–MS heating ramp. In contrast to the other samples, the PBMA/γ-alumina sample did not exhibit a low temperature weight loss that could be attributed to head-to-head chain scission. Apparently, strong interactions between PBMA and γ-alumina prevented unzipping after head-to-head linkage scission for this sample. The weight loss for this sample above 450°C was due primarily to water loss from the oxide. However, Figure 5 shows that alkyl aromatics evolution also contributed to weight loss near 600°C. Relative to the total ion current, the alkyl methacrylates ion signal obtained for the PBMA/γ-alumina sample was considerably less than those for the other samples. This is in agreement with the pyr-GC/MS results (Table I), which show that the PBMA/γ-alumina sample pyrolysis generated considerably less butyl methacrylate than the other PBMA/oxide samples. In contrast to the other PBMA/oxide samples, the alkyl methacrylates ion signal temperature profile for the PBMA/γ-alumina sample exhibited a single peak that appeared above 350°C (Fig. 5), suggesting that weight loss detected below 350°C was not caused by depolymerization. The large quantities of butene detected below 350°C suggests that ester decomposition was the predominant low temperature decomposition process for the PBMA/γ-alumina sample.

VT-DRIFTS results revealed that considerable anhydride was formed by the PBMA/oxide samples, whereas very little was detected for the neat polymer. Unlike the other PBMA/oxide samples, VT-DRIFTS analysis of the PBMA/γ-alumina sample revealed carboxylate formation that maximized at about 470°C. Except for the PBMA/γ-alumina sample, TG–MS ion signal temperature profiles for the PBMA/oxide samples indicated that methacrylic acid evolution was coincident with butene evolution. Methacrylic acid was not detected as a volatile product by TG–MS analysis of the PBMA/γ-alumina sample, and the amount of methacrylic acid detected by pyr-GC/MS analysis of this sample was significantly less than that expected from the large amount of butene evolved from this sample. The formation of carboxylate anions by the PBMA/γ-alumina sample likely accounts for the diminished amount of anhydride detected for this sample by VT-DRIFTS compared to the other PBMA/oxide samples. In fact, Figure 8 indicates that carboxylate appeared in VT-DRIFTS spectra at about the same temperature as butene was first detected by TG–MS analysis of the PBMA/γ-alumina sample. Apparently, poly(methacrylic acid) segments formed on γ-alumina readily deprotonated to form carboxylate anions, whereas anhydride formation was the dominant reaction for poly(methacrylic acid) segments on the other

Table II Kinetic Parameters for Neat PBMA and PBMA/Oxide Depolymerization

PBMA Sample	T_M (°C)	E_A (kcal/mol)	A (s^{-1})
PBMA in He	354	25.5 ± 4.0	$4.9 \times 10^6 \pm 1.0 \times 10^6$
PBMA in He/H_2O	342	26.0 ± 1.3	$1.0 \times 10^7 \pm 7.1 \times 10^5$
Silica in He	381	45.2 ± 1.9	$1.2 \times 10^{13} \pm 7.7 \times 10^{11}$
Silica in He/H_2O	367	53.0 ± 5.3	$1.5 \times 10^{16} \pm 2.7 \times 10^{15}$
Mullite in He	362	35.7 ± 1.8	$1.6 \times 10^{10} \pm 1.1 \times 10^9$
Mullite in He/H_2O	356	39.7 ± 0.9	$5.5 \times 10^{11} \pm 2.7 \times 10^{10}$
α-Alumina in He	372	40.3 ± 0.4	$3.8 \times 10^{11} \pm 5.9 \times 10^9$
α-Alumina in He/H_2O	362	45.5 ± 3.1	$5.0 \times 10^{13} \pm 4.9 \times 10^{12}$
γ-Alumina in He	403	47.0 ± 1.9	$2.2 \times 10^{13} \pm 1.6 \times 10^{12}$
γ-Alumina in He/H_2O	394	47.6 ± 2.0	$4.0 \times 10^{13} \pm 3.1 \times 10^{12}$

oxides. This suggests that the basicity of the γ-alumina surface was greater than that of the other oxides.

Table II lists T_M values and kinetic parameters derived from TG–MS mass spectral data for the primary PBMA depolymerization processes by using the technique of linear programmed thermal degradation mass spectrometry.[26] The considerably larger activation energies obtained for the PBMA/oxide samples compared to those calculated for neat PBMA were reflected in the higher T_M values measured for the PBMA/oxides relative to those for the neat polymer. Table II also indicates that PBMA depolymerization T_M values were reduced in the presence of water vapor even though activation energies for this process were not significantly affected. This effect was greatest for the neat PBMA and PBMA/silica samples. The T_M values and kinetic parameters associated with butene evolution determined for the PBMA/oxide samples by using butene specific m/z 56 ion signal temperature profiles are listed in Table III. Errors associated with the butene evolution kinetic parameters were much larger than those calculated for PBMA depolymerization because the butene ion signal temperature profiles were of lower signal-to-noise ratio than the alkyl methacrylates ion signal temperature profiles. The presence of water vapor during TG–MS analysis affected all butene evolution activation energies but significantly affected T_M values for only the PBMA/silica and PBMA/mullite samples. A comparison of the PBMA depolymerization and ester decomposition T_M values reveals that depolymerization was favored over ester decomposition during TG–MS analysis of the PBMA/silica, PBMA/mullite, and PBMA/α-alumina samples. For these samples, depolymerization T_M values were 25–45°C lower than the ester decomposition T_M values. However, for the PBMA/γ-alumina sample, the opposite trend was observed. For this sample, the T_M value for ester decomposition was about 40°C lower than that for depolymerization.

TG–MS ion signal temperature profiles for alkyl aromatic species derived from the PBMA/oxide samples indicated that the formation of these species maximized 50–70°C higher than the temperature corresponding to the maximum rate of monomer production. Apparently, primary PBMA thermal degra-

Table III Ester Decomposition Kinetic Parameters for Neat PBMA and PBMA/Oxides

PBMA Sample	T_M (°C)	E_A (kcal/mol)	A (s^{-1})
PBMA in He	384	22.6 ± 0.5	$1.6 \times 10^5 \pm 4.6 \times 10^3$
PBMA in He/H_2O	384	27.3 ± 0.5	$6.9 \times 10^6 \pm 1.9 \times 10^5$
Silica in He	411	51.7 ± 7.3	$3.3 \times 10^{14} \pm 6.4 \times 10^{13}$
Silica in He/H_2O	401	39.6 ± 4.9	$5.0 \times 10^{10} \pm 1.1 \times 10^{10}$
Mullite in He	409	53.9 ± 9.7	$1.9 \times 10^{15} \pm 4.7 \times 10^{14}$
Mullite in He/H_2O	402	45.3 ± 0.8	$4.1 \times 10^{12} \pm 1.6 \times 10^{11}$
α-Alumina in He	393	68.6 ± 10.8	$4.3 \times 10^{20} \pm 9.6 \times 10^{19}$
α-Alumina in He/H_2O	393	34.0 ± 6.5	$1.0 \times 10^9 \pm 2.8 \times 10^8$
γ-Alumina in He	360	63.2 ± 2.4	$9.9 \times 10^{19} \pm 7.1 \times 10^{18}$
γ-Alumina in He/H_2O	358	85.7 ± 10.1	$8.0 \times 10^{27} \pm 1.7 \times 10^{27}$

dation processes yielded polyene segments in the residue that subsequently formed volatile aromatic species. These polyene segments were most stable for the PBMA/γ-alumina sample, for which volatile aromatic species were detected by TG–MS at 600°C.

CONCLUSIONS

Although results from the experiments described here were not sufficient to unequivocally identify PBMA thermal degradation mechanisms, these results and our previous results describing the ceramic binder burnout properties of poly(vinyl butyral) (PVB)[13] suggest that binder burnout mechanisms are heavily dependent on the nature of inorganic oxide surfaces and polymer functionalities. Like PVB, PBMA pyr-GC/MS results presented here indicated that significantly more alkyl aromatic species were formed from polymer/oxide samples than from the neat polymer. Detection of volatile alkyl aromatics at temperatures above those at which most of the polymer degraded suggests that unsaturated polymer residue remains during the early stages of ceramic sintering when these polymers are employed as binders, which can ultimately result in flawed ceramic products. Unlike PVB, PBMA thermal degradation was inhibited by the oxides used in this study. The greatest inhibiting effect on polymer degradation was observed for the PBMA/γ-alumina sample, and PBMA degradation occurred most readily when no oxide was present. Unlike PVB, PBMA anhydride moieties (and carboxylate for the PBMA/γ-alumina sample) found in the PBMA residue required higher temperatures for decomposition than the original polymer. Based solely on binder burnout temperature ranges, PVB is clearly more suitable as a ceramic sintering binder than PBMA. However, PVB application requires the use of chlorinated solvents, whereas PBMA is typically applied in 70/30 water–isopropyl alcohol emulsions during manufacture of ceramic green bodies. Chlorinated hydrocarbons are not desired for use in manufacturing processes because of their adverse environmental consequences. Therefore, although the burnout characteristics of PVB are clearly superior to those of PBMA, PBMA is still an attractive ceramic binder for nonoxidative sintering because manufacturing with this polymer results in fewer environmental problems.

Financial support for this work from Hitachi, Ltd. is gratefully acknowledged.

REFERENCES

1. K. Otsuka, T. Usami, and M. Sekibata, *Yogyo Kyokaishi,* **89,** 309 (1981).
2. K. Otsuka and S. Ogihara, *Yogyo Kyokaishi,* **92,** 210 (1984).
3. K. Otsuka and S. Ogihara, *Yogyo Kyokaishi,* **92,** 629 (1984).
4. K. Otsuka and S. Ogihara, *Yogyo Kyokaishi,* **93,** 28 (1985).
5. H. W. Stetson, *High Technology Ceramics—Past, Present and Future, Ceramics and Civilization Ser.,* Vol. 3, American Ceramic Society, Westerville, OH, 1986 p. 307.
6. M. J. Cima and J. A. Lewis, *Ceram. Trans.,* **1,** 567 (1988).
7. Y. N. Sun, M. D. Sacks, and J. W. Williams, *Ceram. Trans.,* **1,** 538 (1988).
8. M. J. Cima, J. A. Lewis, and A. D. Devoe, *J. Am. Ceram. Soc.,* **72,** 1192 (1989).
9. S. Masia, P. D. Calvert, W. E. Rhine, and H. K. Bowen, *J. Mater. Sci.,* **24,** 1907 (1989).
10. R. L. White and A. Nair, *Chem. Mater.,* **2,** 742 (1990).
11. R. L. White and J. Ai, *Chem. Mater.,* **4,** 233 (1992).
12. J. Ai, L. L. Phegley, G. Christen, and R. L. White, *J. Am. Ceram. Soc.,* **78,** 874 (1995).
13. A. Nair and R. L. White, *J. Appl. Polym. Sci.,* **60,** 1901 (1996).
14. T. Kashiwagi, A. Inaba, J. E. Brown, K. Hatada, T. Kitayama, and E. Masuda, *Macromolecules,* **19,** 2160 (1986).
15. J. Song, C. H. Fischer, and W. Schnabel, *Polym. Degrad. Stab.,* **36,** 261 (1992).
16. L .E. Manring, *Macromolecules,* **24,** 3304 (1991).
17. N. Higashi, H.Shiba, and M. Niwa, *Macromolecules,* **22,** 4652 (1989).
18. P. Cacioii, G. Moad, E. Rizzardo, A. K. Serelis, and D. H. Solomon, *Polym. Bull.,* **11,** 325 (1984).
19. W. A. Pryor and K. Smith, *J. Am. Chem. Soc.,* **92,** 5403 (1970).
20. N. Grassie, *Pure Appl. Chem.,* **30,** 119 (1972).
21. N. Grassie and J. G. Speakman, *J. Polym. Sci., Part A: Polym. Chem.,* **9,** 919 (1971).
22. J. K. Haken and L. Tan, *J. Polym. Sci., Part A: Polym. Chem.,* **26,** 1315 (1988).
23. P. K. Dhal and G. N. Babu, *J. Polym. Sci., Polym. Chem. Ed.,* **22,** 1817 (1984).
24. R. A. Divis and R. L. White, *Anal. Chem.,* **61,** 33 (1989).
25. Y. N. Sun, M. D. Sacks, and J. W. Williams, *Ceram. Trans.,* **1,** 538 (1988).
26. T. H. Risby and A. L. Yergey, *Anal. Chem.,* **50,** 326A (1978).

Received August 10, 1995
Accepted December 6, 1995